J Solid State Electrochem
DOI 10.1007/s10008-016-3347-8

ORIGINAL PAPER

Properties of composites of metal hydride alloys synthesized by mechanical milling

R. M. Humana[1,2] · F. C. Ruiz[3] · J. E. Thomas[4] · H. A. Peretti[3] · E. B. Castro[4] · A. Visintin[4]

Received: 12 April 2016 / Revised: 25 July 2016 / Accepted: 29 July 2016

Abstract Hydride-forming alloys are used as negative electrode components of nickel metal hydride (MH) batteries. Generally, commercially used compounds are made of two types of alloys, rare earth based on $LaNi_5$, known as AB_5 type, and alloys based on $ZrCr_2$, ZrV_2, $ZrMn_2$, and $TiMn_2$, known as AB_2 type (Laves phases). A and B are generally composed of more than one element. In both systems, the A components are metals that form stable hydrides, while the B components are transition metals and form less stable hydrides. In the present work, electrodes were prepared using composite material obtained by mechanical milling of different proportions of $ZrTiV_{0.8}Ni_2Cr_{0.52}Mn_{0.56}Co_{0.08}Al_{0.04}$ (AB_2) and $LaNi_{3.6}Co_{0.7}Mn_{0.4}Al_{0.3}$ (AB_5) alloys. The particles of the AB_5 alloy were dispersed on the surface of the AB_2 particles, as shown by scanning electron microscopy (SEM) and energy-dispersive spectrometry (EDS). The discharge capacity of the electrodes improved with the addition of 80 and 50 weight-% AB_2. The maximum discharge capacities obtained, after 30 cycles, for electrodes with 50 and 80 % AB_2 were above 200 mA h g^{-1}, while for the original AB_2 alloy it was less than 170 mA h g^{-1}. A decrease in the composite concentration of the AB_2 alloy improves the exchange current density, as can be seen from electrochemical impedance spectroscopy (EIS) measurements. High-rate dischargeability (HRD) and EIS results showed enhanced hydrogen diffusion for the samples with an AB_2 concentration of 50 and 80 %.

Keywords Metal hydride · Ni/MH batteries · Ball milling · Electrochemical properties

E. B. Castro passed away in 2013

✉ A. Visintin
avisintin@inifta.unlp.edu.ar

[1] Centro de Investigaciones y Transferencia de Catamarca (CITCA), CONICET-UNCA, Prado 366, K4700AAP, San Fernando del Valle de Catamarca, Catamarca, Argentina

[2] Facultad de Ciencias Exactas y Naturales, UNCA, Av. Belgrano N° 300, 4700 Catamarca, Argentina

[3] Centro Atómico Bariloche (CAB), Comisión Nacional de Energía Atómica (CNEA), Instituto Balseiro–Universidad Nacional de Cuyo (IB-UNCu), CONICET, Av. Bustillo 9500 CAB, 8400 San Carlos de Bariloche, Argentina

[4] Instituto de Investigaciones Fisicoquímicas Teóricas y Aplicadas (INIFTA), Facultad de Ciencias Exactas y Naturales, UNLP, CCT La Plata-CONICET, C.C. 16, Suc. 4, 1900 La Plata, Argentina

Introduction

Hydrogen can be stored as (i) pressurized gas, (ii) cryogenic liquid, or (iii) solid fuel as a chemical or physical combination with materials such as metal hydrides, complex hydrides, and carbon materials [1]. Hydrogen forms metal hydrides with some metals and alloys, allowing solid state storage at moderate temperature and pressure, which is an important safety advantage over the gas and liquid storage techniques [2].

Metal hydride alloys are mostly used as materials for negative electrodes in alkaline rechargeable cells and hydrogen storage. The principles on which NiMH cells operate are based on their ability to absorb, release, and transport hydrogen between the electrodes within the cell. When a NiMH cell is charged, the positive electrode releases hydrogen into the electrolyte. The hydrogen is then absorbed and stored in the negative electrode. Metal hydrides are formed by transition metals including the rare earth and actinide series. They have high thermal and electrical conductivities. However, unlike metals, they are quite brittle. Metal hydrides have a wide variety of stoichiometric and non-stoichiometric compounds and

Published online: 10 August 2016

are formed by direct reaction of hydrogen with the metal or by electrochemical reaction [3].

There are basically two types of binary compounds that make up the majority of the nickel metal hydride battery market; AB_2-type and AB_5-type compounds. The basic crystal structure is of the layered hexagonal $CaCu_5$ type [4]. The AB_2 compounds form one of two structures, either the cubic C15 structure or the hexagonal C14 one [4–6]. In this notation, A represents a metallic element with a strong affinity to hydrogen, whereas B is a metallic element with weak hydrogen affinity (typically a transition metal) [7].

The hydrogen evolution reaction is one of the most often studied electrocatalytic reactions. It is well accepted that the reaction mechanism in alkaline solutions usually proceeds through three steps: (1) electroreduction of water with adsorption of hydrogen, the Volmer reaction (Eq. 1), and two possible desorption steps: (2) electrochemical desorption of hydrogen, the Heyrovský reaction (Eq. 2), and (3) chemical desorption, the Tafel reaction (Eq. 3) [8]:

$$H_2O + M + e^- \underset{k_{-1}}{\overset{k_1}{\rightleftarrows}} MH_{ad} + OH^- \quad (1)$$

$$MH_{ad} + H_2O + e^- \underset{k_{-2}}{\overset{k_2}{\rightleftarrows}} M + H_2 + OH^- \quad (2)$$

$$2MH_{ad} \underset{k_{-3}}{\overset{k_3}{\rightleftarrows}} 2M + H_2 \quad (3)$$

The constant search for new hydride-forming materials with suitable composition and structure, which have a good performance as negative electrodes in NiMH batteries, remains a research topic and has led to the development of different preparation methods for these materials. Mechanical alloying, usually carried out under argon atmosphere in a ball mill, is an alternative to the traditional method in which the production of materials is carried out by high-temperature synthesis. Ball milling is a very effective technique for modifying the surface, structure, and properties of intermetallic alloys in order to improve their characteristics for hydrogen storage applications [9–16]. Recent studies suggest that the best mixed materials can have good hydrogen storage characteristics and play an important role in accelerating the hydriding process [17, 18]. Some investigations reported that the AB_2/AB_5 composite alloys exhibit the best behavior for hydrogen storage [19, 20].

In the mechanical alloying process, a blend of powders is subjected to highly energetic compressive impact forces. The process involves repeated deformation, fracture, and welding of the particles. The nature of these processes depends on the mechanical behavior of the powder components, phase equilibrium, and the state of stress during grinding.

The aim of the present work is to study the electrochemical properties of mixed compounds prepared from AB_2 and AB_5 alloy types using mechanical milling as mixing method. The electrochemical results were also examined using a physicochemical model based on the theory of porous electrodes [21–27].

Experimental

Preparation of alloys and composites

The AB_5 and AB_2 alloys were prepared by arc melting in a cooled copper crucible under argon atmosphere using the constituent elements with a purity of >99.9 %, obtaining buttons, about 20 g each, of each alloy. The final stoichiometry of the alloy buttons, after melting, was $LaNi_{3.6}Co_{0.7}Mn_{0.4}Al_{0.3}$ and $ZrTiV_{0.8}Ni_2Cr_{0.52}Mn_{0.56}Co_{0.08}Al_{0.04}$, respectively.

The AB_5 and AB_2 alloy buttons were mechanically crushed and mixed in the 80:20, 50:50, and 20:80 weight ratios and milled in an Spex 8000D ball mill under argon atmosphere for 30 min. A ball/sample mass ratio of 8.3 was selected. Ball milling offers the possibility to combine two or more alloys having different characteristics [28, 29]. The milling time was sufficient to prepare a homogeneous mixture between the alloys, and the samples were structurally stable. Also, powders from AB_2 and AB_5 samples were milled separately under the same conditions and used as pure alloys. The final material used to prepare electrodes and its composition are indicated and labeled in Table 1.

Material characterization

The structural changes of the alloys were characterized by XRD (Philips PW1700). The morphology of the sample was examined by a scanning electron microscope (Philips, model 515 SEM) coupled with an energy-dispersive X-ray spectrometer (EDAX Genesis 2000).

The electrodes were built as described in [27]. All electrochemical measurements were performed in a three-compartment cell consisting of a working electrode, NiOOH counterelectrode, and Hg/HgO reference electrode. The

Table 1 Labels and compositions of the prepared samples

Label	Composition
M100	$AB_5/AB2$ 0:100 *w/w*
M80	AB_5/AB_2 20:80 *w/w*
M50	AB_5/AB_2 50:50 *w/w*
M20	AB_5/AB_2 80:20 *w/w*
M0	AB_5/AB_2 100:0 *w/w*

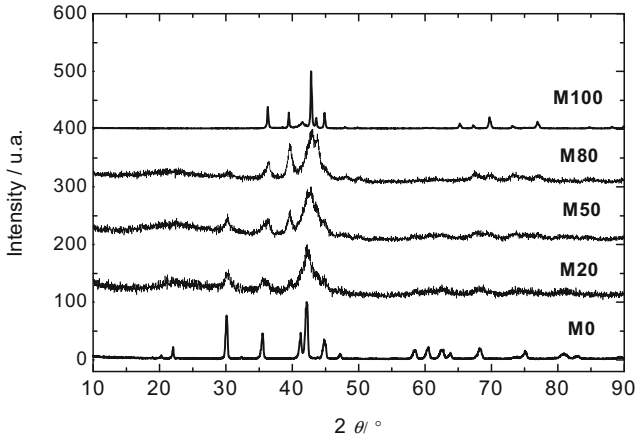

Fig. 1 Diffraction patterns of M100, M80, M50, M20, and M0 samples

electrolyte was a 6-M KOH solution. All the potentials are referred to the Hg/HgO reference electrode.

Electrochemical measurements

The working electrodes were charge-discharge cycled at constant current until a constant hydrogen storage capacity was obtained. During charge-discharge experiments, constant currents of −10 and 10 mA, respectively, were applied. Following a charging time of 4 h, a cutoff potential of −0.6 V was used for discharge. The measurements were performed at a controlled temperature of 30 °C. The rate capability performance of the cells was studied at different currents (2.5, 10, 15, 30, 45, 60, 75, and 90 mA) during 3 cycles. The scan rate of cyclic voltammogram (CV) measurements was 1 mV s^{-1} between −1.2 and −0.6 V. Electrochemical impedance spectroscopy (EIS) measurements were carried out at a constant potential corresponding to 50 % state of charge (SOC). The spectra were recorded in the

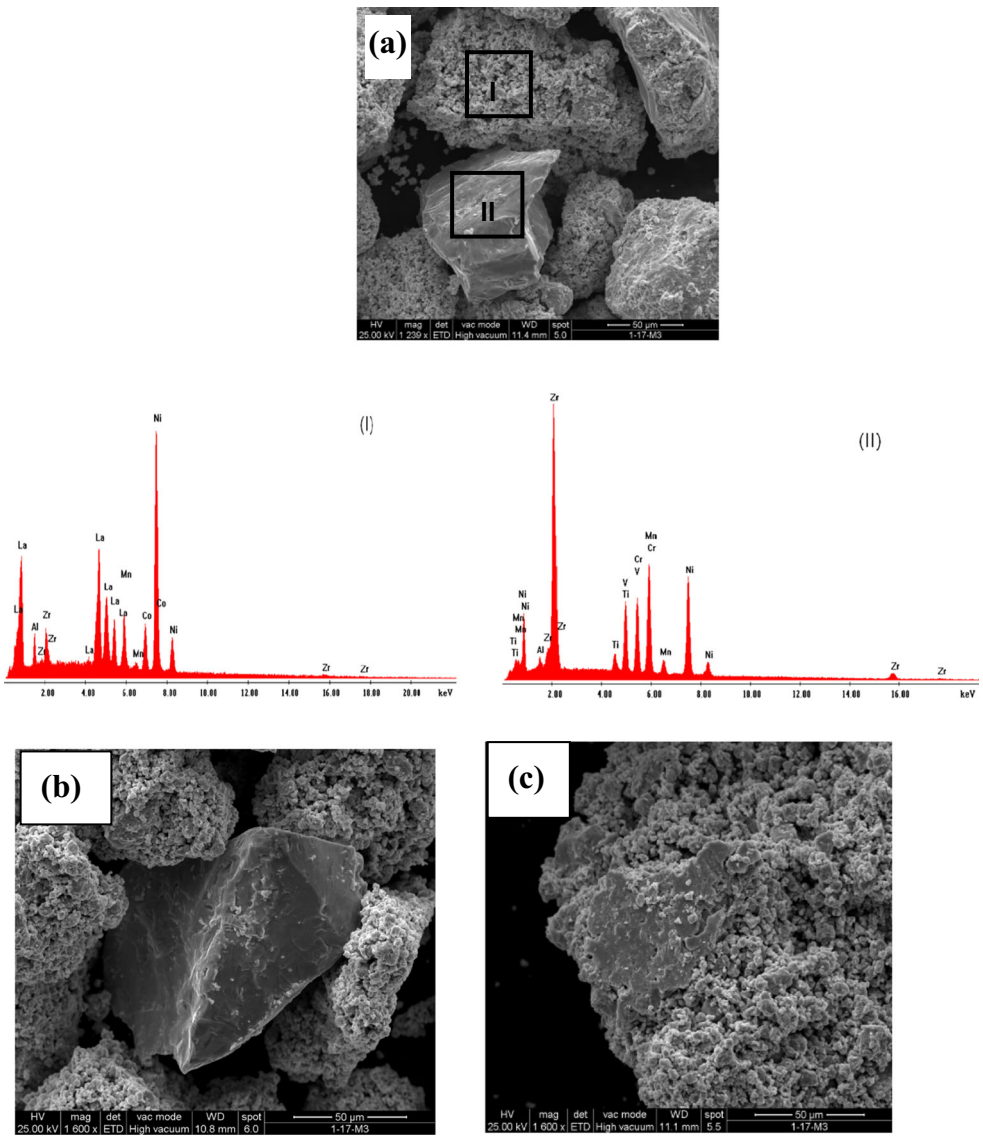

Fig. 2 SEM images and EDS patterns of **a** M20, **b** M50, **c** M80

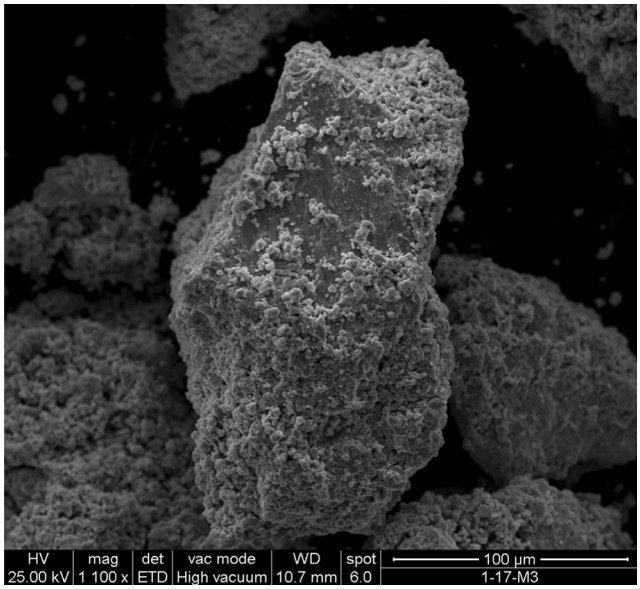

Fig. 3 SEM images and EDS patterns of M50 show that the small particles on the alloy surface are adhered to the bulk of AB_2 alloy particles

frequency range 0.1–10.000 Hz with an amplitude of 5 mV. Experimental data obtained from EIS measurements were adjusted in terms of a physicochemical model described in [21–27].

Results and discussion

Metallurgical characterization

The XRD patterns of ball-milled M100, M80, M50, M80, and M0 composite alloys are shown in Fig. 1. It was found that sample M100 can be indexed as the hexagonal C14 Laves phase. For each single unmixed alloy, the peaks were well defined and, as the concentration of AB_5 increases, some peaks started to disappear. The M80 composite tends to have

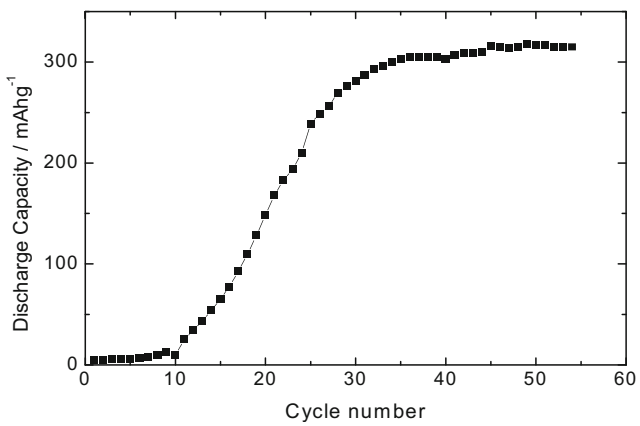

Fig. 4 Discharge capacity versus cycle number for the AB_2 alloy electrode without the ball milling process at 10 mA

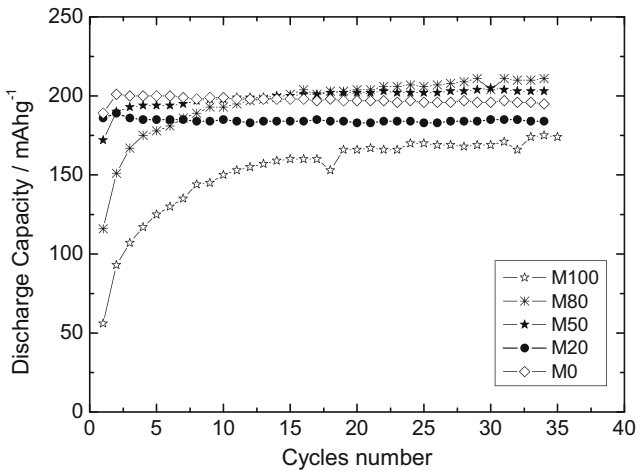

Fig. 5 Discharge capacity versus cycle number for different electrodes at 10 mA

a similar structure to that of the AB_2 alloy, and therefore, its properties were expected to be similar.

In samples obtained from AB_2 and AB_5 alloy mixtures, an increase of the peak width and a simultaneous decrease in intensity were observed, which revealed a decrease of the average crystallite size that can be attributed to an increase of the internal stress introduced by mechanical deformation. This indicates that the alloy underwent a conversion process passing from the crystalline state to the amorphous state. Furthermore, the ball milling technique is very effective to modify the structure and surface properties.

The SEM images and EDS patterns of ball-milled M20, M50, and M80 composites are shown in Fig. 2. In the case of the M20 sample, as shown in Fig. 2a, the different EDS patterns of area (I) and (II) indicate that the small particles consist of AB_5, while the big ones are composed of AB_2.

Figure 3 shows that the small particles on the alloy surface are adhered to the bulk of AB_2 alloy particles. The AB_5 alloy particles were pulverized more easily and adhered to the

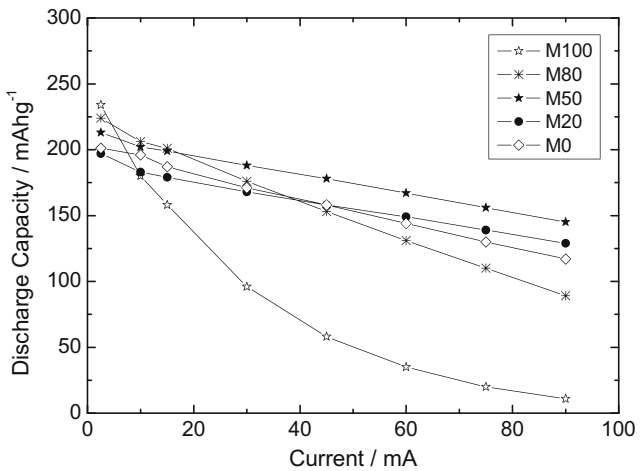

Fig. 6 Discharge capacity versus discharge current for different electrodes

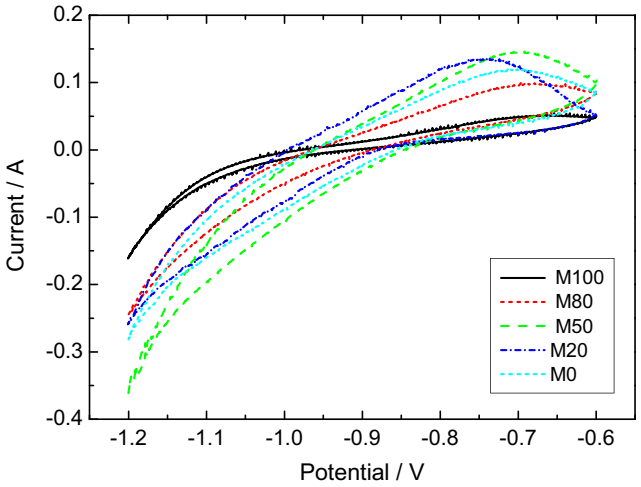

Fig. 7 Cyclic voltammograms of the alloys and composites

surface of the larger AB_2 alloy particles due to the different hardness and ductility of the two alloys [30].

The mechanical alloying process creates fresh surfaces during processing. This provided a larger available surface area for electrochemical reactions. Particles having a rough surface provide a greater contact surface between them and therefore may favor agglomeration. This effect has been shown in previous studies [18, 30].

Electrochemical characterization

For comparison, Fig. 4 shows the electrochemical behavior of an electrode prepared without the ball milling process of AB_2 alloy, under the same working conditions. The activation of an electrode is defined as the number of charge-discharge cycles required to reach maximum capacity. The activation of the metal alloy plays a key role in the electrode absorption/desorption process, since it defines the reaction rate of hydrogen with the metal and the incorporation of hydrogen into the bulk structure of the metal [3, 4]. The surfaces of alloys are usually covered with a passive oxide film of various thicknesses, depending on the formation process of each particular alloy. This oxide layer acts as a hydrogen barrier and must be broken during the first cycles in order to allow hydrogen access to the bare metal [3, 18, 25]. The activation time was longer, and the maximum hydrogen storage capacity obtained was 300 mA h g^{-1} in the 35th cycle. Figure 5 shows that the electrodes prepared with the alloys obtained by ball milling reach the maximum hydrogen storage capacity in the first cycles. It can be observed that the activation time decreases remarkably with this type of milling in the case of AB_2.

The increment of the discharge capacities of M50 and M80 electrodes can be attributed to the increase in catalytic activity on the alloy surface. This can be due to an increase of the Ni concentration [31]. The discharge capacity enhancement is attributed to the added AB_5 alloy particles on the surface layer of M20, M50, and M80 samples.

The decrease in storage capacity can be attributed to the possible formation of an oxide film that would prevent hydrogen from entering the particle [18]. Although samples are prepared under inert atmosphere, contamination may come from the air before the electrodes are measured.

Figure 6 shows the relationship between the discharge capacity and discharge current of the electrodes. It can be noticed that the discharge capacity decreased as the discharge current (I_d) increases. This effect was at maximum for the single AB_2 intermetallic alloy, while for the mixed alloys, the high-rate dischargeability (HRD) decrease was less pronounced and close to the one of single AB_5.

Moreover, the performance of the electrodes with 20 and 50 % AB_2 was better than that of the electrodes with 100 % AB_5 and 100 % AB_2. The electrocatalytic and/or transport properties improved for the electrodes with composite mixtures.

A similar response was observed by cyclic voltammetry (Fig. 7). The peak height and area increased as the AB_2 content in the samples decreased, indicating an improvement in the electrochemical kinetics and discharge capacity.

Figure 7 shows cyclic voltammograms of the M100, M80, M50, M20, and M0 electrodes. In each alloy sample, the oxidation peak appears at about −0.75 V. This peak was

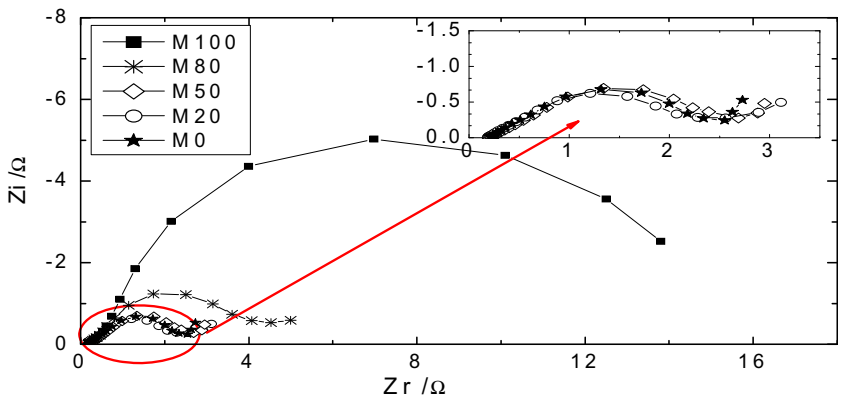

Fig. 8 Electrochemical impedance spectra of the M100, M80, M50, M20, and M0 alloy electrodes at 50 % SOD

attributed to hydrogen desorption from the interior of alloy particles. The adsorption of hydrogen atoms on the electrode and the hydrogen evolution reaction at the electrode surface give a simple reduction peak at −1.2 V, overlapped by the hydrogenation of the alloy particle and hydrogen gas evolution. It is not possible to separate the contribution of each reaction, since they take place at the same potentials.

These results indicate that in composites with AB_2 contents of up to 50 %, the discharge capacity and the reaction kinetics improved with respect of that of the single AB_5 alloy. These results are in good agreement with HRD and EIS measurement results.

Figure 8 shows Nyquist EIS plots, at 50 % state of discharge (SOD) of alloys and composites, respectively. The plots exhibit a linear behavior in the high-frequency range with a slope of approximately 45°, a typical response associated with a porous structure. A semicircle that corresponds to the charge transfer resistance appears at intermediate frequencies. At low frequency, a Warburg-type response, associated with the hydrogen diffusion process, can be seen. In the same frequency range, such response is absent in the electrodes with a high percentage of AB_2-type alloy. A lower composite concentration of AB_2 alloy decreased the charge transfer resistance of the electrodes.

From the fitting procedure of EIS data in terms of the physicochemical model based on the classic theory of porous flooded electrodes [21–27], this accounts for the charge-discharge process taking place at the active material/electrolyte interface of the electrode porous structure. A good agreement between experimental and theoretical results is shown in Fig. 9a–e.

From the fitting procedure, similar values of the diffusion coefficient (D_H) and exchange current density (i_o) were obtained for all electrodes (Table 2).

According to all results, the better voltammetry and HRD responses obtained with electrode M50 indicate that the addition of AB_2 by mechanical milling allows improving the

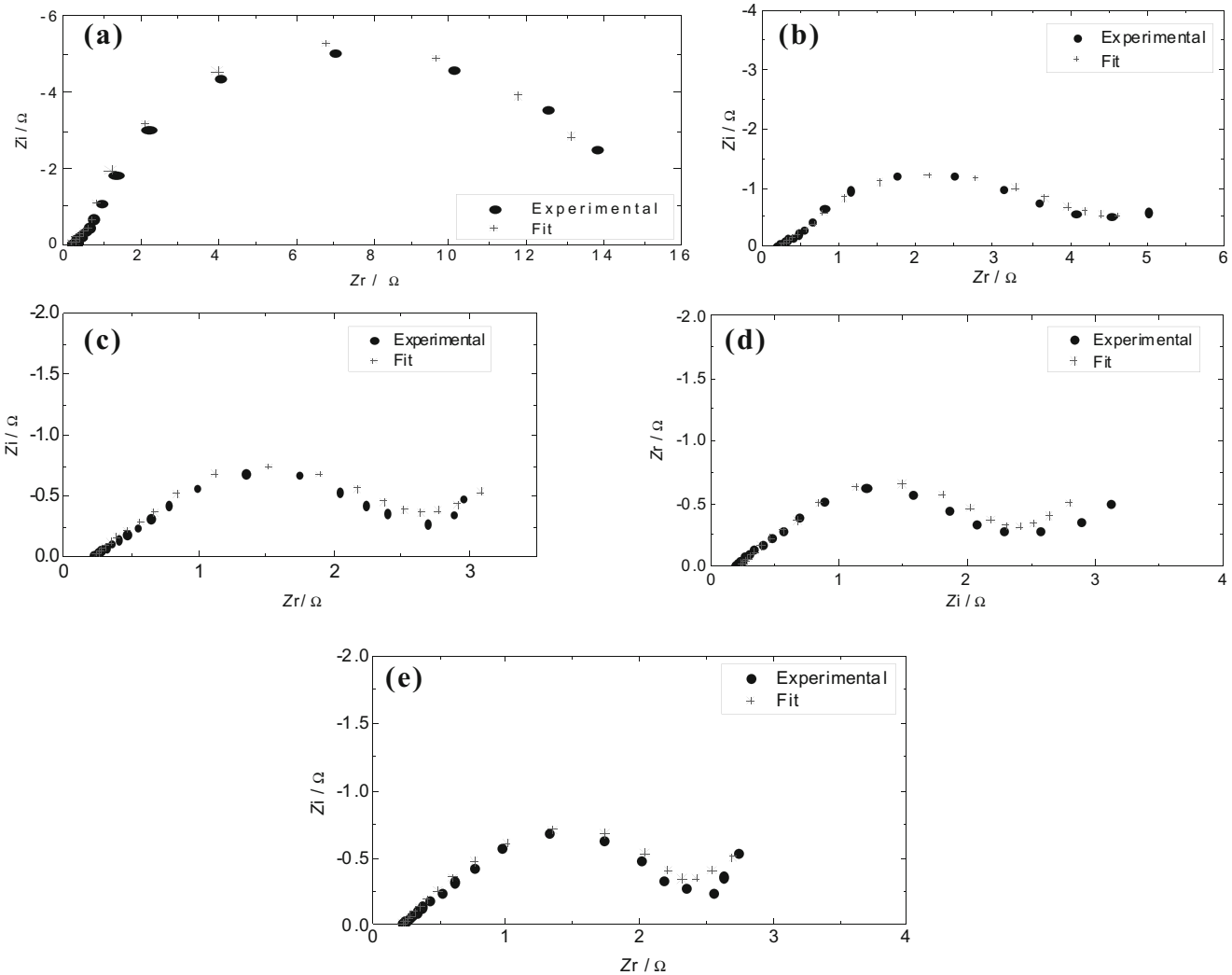

Fig. 9 Experimental and theoretical impedance spectra of the electrodes: **a** M100, **b** M80, **c** M50, **d** M20, **e** M0

Table 2 Parameter values, derived from the fitting procedure, for the electrodes

	Alloy	i_o (A cm^{-2})	D_H (cm^2 s^{-1})	k_2 (mol s^{-1} cm^{-2})	A_a (cm^{-1})	K (Ω^{-1} cm^{-1})	R_a (cm)	A_i (cm^{-1})
M100	AB2	1.2×10^{-4}	$4.0\ 10^{-16}$	7.1×10^{-11}	517	0.1	7.0×10^{-4}	4.8×10^{4}
M80	AB2	1.0×10^{-4}	4.0×10^{-16}	7.1×10^{-11}	1500	0.1	3.0×10^{-4}	1.1×10^{5}
	AB5	7.0×10^{-4}	1.2×10^{-10}	0	20		1.0×10^{-3}	
M50	AB2	1.0×10^{-4}	4.0×10^{-16}	7.1×10^{-11}	1500	0.1	3.0×10^{-4}	1.1×10^{5}
	AB5	7.0×10^{-4}	1.2×10^{-10}	0	80		1.0×10^{-3}	
M20	AB2	1.0×10^{-4}	4.0×10^{-16}	7.1×10^{-11}	1500	0.1	3.0×10^{-4}	1.1×10^{5}
	AB5	7.0×10^{-4}	1.2×10^{-10}	0	100		1.0×10^{-3}	
M0	AB5	7.0×10^{-4}	1.2×10^{-10}	0	172	0.08	1.4×10^{-3}	1.7×10^{5}

utilization of the active material. It is apparent that electrode surfaces modified by mechanical milling increase the active surface. This increases the conducting network and consequently the discharge depth of active materials.

Table 2 lists the physicochemical and structural parameters derived from the fitting procedure.

The parameters Γ (maximum surface concentration of H_{ad}), C_{dl} (double layer capacitance), and C_{max} (maximum H concentration in the alloy) were considered constant according to previous publications [26, 27]. For the electrodes M20, M50, and M80, the values D_H, i_o, *Ra* (average radius of alloy particles), and *Aa* (active area per electrode unit volume) were obtained for each alloy.

Parameters (i_o, D_H, k_2) obtained by fitting the data on electrodes M0 and M100 were used to adjust the composite electrodes. The *Aa* value increased as a result of an increase in the concentration of the AB_5 electrode. For AB_2 alloys, the D_H value is much lower than in AB_5 alloys, marking an important difference between the two alloys, which accounts for the behavior observed in HRD and EIS responses. The value of interfacial area per unit volume (A_i) is relatively constant. This parameter is mainly related to the area of carbon particles and is not influenced by the particles of different alloys.

For AB_5 alloy electrodes, the kinetic constant of the Heyrovský reaction (k_2) from Eq. 2 was not identifiable, due to the prevalence of the H absorption process over H_2 evolution [32].

Conclusion

The electrochemical properties of composite materials of electrodes prepared by mechanical alloying of different proportions of AB_2- and AB_5-type alloys were analyzed. Mechanical milling resulted in a reduction of the particle size and changes of particle shape, which facilitates hydrogen desorption from the alloys. The electrodes prepared with the alloys obtained by this method reached the maximum hydrogen storage capacity in the first cycles. SEM images indicated that small particles resulting from the crushing of the brittle AB_5 alloy adhered to the larger and ductile particles remaining from the AB_2 alloy. Electrochemical results revealed that the discharge capacity of the electrodes improved with the addition of the AB_2 alloy, providing a better performance with the addition of 80 and 50 weight-%. Also, the HRD and EIS results showed enhanced hydrogen diffusion for the samples with an AB_2 concentration of 50 and 80 %.

Acknowledgments This work was supported by Agencia Nacional Promoción Científica y Tecnológica of Argentina, Consejo Nacional de Investigaciones Científicas y Técnicas (CONICET), Universidad Nacional de Catamarca and Universidad Nacional de La Plata.

References

1. Ogden JM (1999) Developing an infrastructure for hydrogen vehicles: a Southern California case study. Int J Hydrog Energy 24:709–730
2. Sakintuna B, Lamaridarkrim F, Hirscher M (2007) Metal hydride materials for solid hydrogen storage: a review. Int J Hydrog Energy 32:1121–1140
3. Hirscher M (2010) Handbook of hydrogen storage: new materials for future energy storage. doi: 10.1002/9783527629800
4. Sandrock G (1999) A panoramic overview of hydrogen storage alloys from a gas reaction point of view. J Alloys Compd 293-295:877–888
5. Ivey DG, Northwood DO (1983) Storing energy in metal hydrides: a review of the physical metallurgy. J Mater Sci 18:321–347
6. Shaltiel D (1978) Hidride properties of AB2 laves phase compounds. J Less-Common Met 62:407–416
7. Züttel A (2003) Materials for hydrogen storage. Mater Today 6:24–33
8. Lasia A (2002) Applications of the electrochemical impedance spectroscopy to hydrogen adsorption, evolution and absorption into metals. In: Conway BE, White RE (eds) Modern aspects of electrochemistry. Springer USA, Berlin Heidelberg New York, pp. 1–49
9. Prasad Yadav T, Manohar Yadav R, Pratap Singh D (2012) Mechanical milling: a top down approach for the synthesis of nanomaterials and nanocomposites. Nanosci Nanotechnol 2:22–48
10. Koch CC, Whittenberge JD (1996) Mechanical milling/alloying of intermetallics. Intermetallics 4:339–355
11. Benjamin JS, Volin TE (1974) The mechanism of mechanical alloying. Metall Trans 5:1929–1934

12. Wright IG, Wilcox BA (1974) Observations on strengthening and oxidation behavior of a dispersion hardened Fe–Cr–Base alloy prepared by mechanical alloying. Metall Trans 5:957–960
13. Benjamin JS (1900) Mechanical alloying—a perspective. Met Powder Rep 45:122–127
14. Zaluski L, Zaluska A, Olsen JOS (1995) Hydrogen absorption in nanocrystalline Mg2Ni formed by mechanical alloying. J Alloys Compd 217:245–249
15. Yu XB, Walker GS, Grant DM, et al. (2005) Electrochemical hydrogen storage of Ti–V-based body-centered-cubic phase alloy surface-modified with AB5 nanoparticles. Appl Phys Lett 87: 133121
16. Yu XB, Dou T, Wu Z, et al. (2006) Electrochemical hydrogen storage in Ti–V-based alloys surface-modified with carbon nanoparticles. Nanotechnol 17:268–271
17. Nagai H, Tomizawa H, Ogasawara T, Shoji K-I (1990) Hydriding characteristics of Mg-xwt.%LaNi5 sintered alloys. J Less-Common Met 157:15–24
18. Jain A, Agarwal S, Vyas D, et al. (2010) Correlation between the milling time and hydrogen storage properties of ZrCrFe ternary alloy. Int J Hydrog Energy 35:9910–9915
19. Han S-M, Zhao M-S, Zhang Z, et al. (2005) Effect of AB2 alloy addition on the phase structures and electrochemical characteristics of LaNi5 hydride electrode. J Alloys Compd 392:268–273
20. Han S, Zhang Z, Zhao M, Zheng Y (2006) Electrochemical characteristics and microstructure of Zr0.9Ti0.1Ni1.1Mn0.6V0.3Zr0.9Ti0.1Ni1.1Mn0.6V0.3–LaNi5LaNi5 composite hydrogen storage alloys. Int J Hydrog Energy 31:563–567
21. Lundqvist A, Lindbergh G (1999) Kinetic study of a porous metal hydride electrode. Electrochim Acta 44:2523–2542
22. Meyers JP, Doyle M, Darling RM, Newman J (2000) The impedance response of a porous electrode composed of intercalation particles. J Electrochem Soc 147:2930–2940
23. Paxton B, Newman J (1997) Modeling of nickel/metal hydride batteries. J Electrochem Soc 144:3818–3831
24. Micka K, Rousar I (1979) Theory of porous electrodes-xvi. The nickel hydroxide electrode. Electrochim Acta 25:1085–1090
25. Visintin A, Castro E, Real S, et al. (2006) Electrochemical activation and electrocatalytic enhancement of a hydride-forming metal alloy modified with palladium, platinum and nickel. Electrochim Acta 51:3658–3667
26. Castro E, Real S, Bonesi A, et al. (2004) Electrochemical impedance characterization of porous metal hydride electrodes. Electrochim Acta 49:3879–3890
27. Humana RM, Thomas JE, Ruiz F, et al. (2012) Electrochemical behavior of metal hydride electrode with different particle size. Int J Hydrog Energy 37:14966–14971
28. Zaluski L, Zaluska A (1997) Nanocrystalline metal hydrides. J Alloys Compd 254:70–79
29. Singh A, Singh BK, Davidson DJ, Srivastava ON (2004) Studies on improvement of hydrogen storage capacity of AB5 type: MmNi4.6Fe0.4 alloy. Int J Hydrog Energy 29:1151–1156
30. Cerón-Hurtado NM, Esquivel MR (2010) Stages of mechanical alloying during the synthesis of Sn-containing AB5-based intermetallics. Int J Hydrog Energy 35:6057–6062
31. Korea S (1997) The hydrogenation characteristics of Ti-Zr-V-Mn-Ni C14 type Laves phase alloys for metal hydride electrodes. J Alloys Compd 254:601–604
32. Castro BE, Milocco RH (2005) Identifiability of sorption and diffusion processes using EIS: application to the hydrogen reaction. J Electroanal Chem 579:113–123